

Chip-on-Board assembly of 800V Si L-IGBTs for high performance ultra-compact LED drivers

A. M. Aliyu, B. Mouawad,
A. Castellazzi
Power Electronics, Machines and
Control Group
University of Nottingham,
Nottingham, United Kingdom

P. Rajaguru, C. Bailey
Computational Mechanics and
Reliability Group
University of Greenwich,
London, United Kingdom

V. Pathirana, N. Udugampola, T.
Trajkovic, F. Udrea
University of Cambridge &
Cambridge Microelectronics Ltd,
Cambridge, United Kingdom

Abstract— This paper presents a novel chip on board assembly design for an integrated power switch, based on high power density 800V silicon lateral insulated gate bipolar transistor (Si LIGBT) technology. LIGBTs offer much higher current densities (5-10X), significantly lower leakage currents, lower parasitic device capacitances and gate charge compared to conventional vertical MOSFETs commonly used in LED drivers. The higher voltage ratings offered (up to 1kV), the development of high voltage interconnection between parallel IGBTs, self-isolated nature and absence of termination region unlike in a vertical MOSFET makes these devices ideal for ultra-compact, low bill of materials (BOM) count LED drives. Chip on-board LIGBTs also offer significant advantages over MOSFETs due to high temperatures seen on most of the LED lamp enclosures as the LIGBT's on-state losses increase only marginally with temperature. The design is based on a built-in reliability approach which focuses on a compact LED driver as a case-study of a cost-sensitive large volume production item.

Keywords—*chip-on-board; lateral IGBT; LED drivers; packaging; reliability.*

I. INTRODUCTION

The semiconductor device design advances state-of-the-art by enabling realisation of significantly more compact solutions in size sensitive products such as LED lighting, mobile phones, implantable cardioverter defibrillators (ICDs) and tablet chargers [1, 2]. The advantage of high current density, low power losses and reduced device footprint has led to an increased attention towards these devices in high voltage low power applications [3]. To match the level of advancement associated with the chip technology and enable the full exploitation of its potential at application level, the assembly exercise targets the structural and functional integration of design elements to yield optimised electrical and thermal management of the chip. The significance of the contribution is: it delivers a methodology for developing highly integrated, reliable and cost-effective lateral Si-based power switches. As far as we are aware, this is the first time the lateral smart integrated chip together with a chip on board assembly are

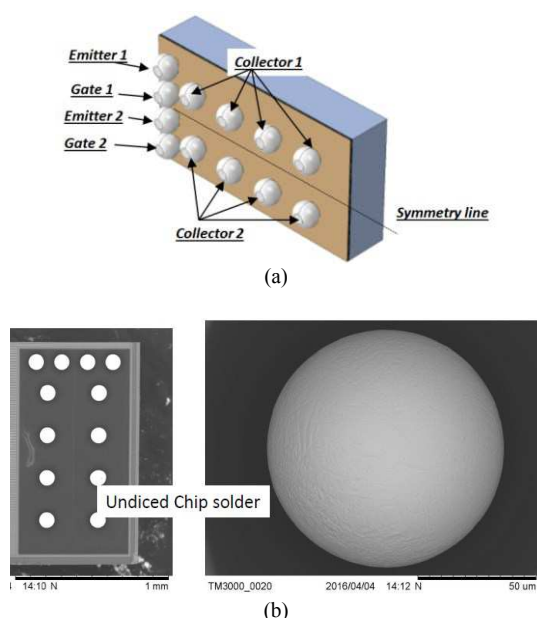


Fig.1: (a) Terminal layout of two identical LIGBTs with a fully populated solder ball matrix on a silicon based substrate (b) scanning electron microscope (SEM) image of the LIGBT and close view of a solder ball

employed in an LED driver. The 3D model of the LIGBT device considered in this work is shown in Fig.1(a). An electron microscope is used capture the image of the device as shown in Fig.1(b). The size of the device is $744\mu\text{m} \times 1345\mu\text{m}$ with the deposited solder balls that has a radius of just above $50\mu\text{m}$. This poses obvious thermal and electrical challenges, which need to be analysed in order to ensure reliable performance.

The layout of the fabricated LIGBT developed in $0.6\mu\text{m}/5\text{V}$ bulk silicon technology is shown in Fig. 2(a). The cross section along A in Fig. 2(a) reveals the 3-dimensional schematic of the LIGBT device structure presented in Fig. 2(b). The LIGBT possesses a new design feature which is a floating N^+ layer

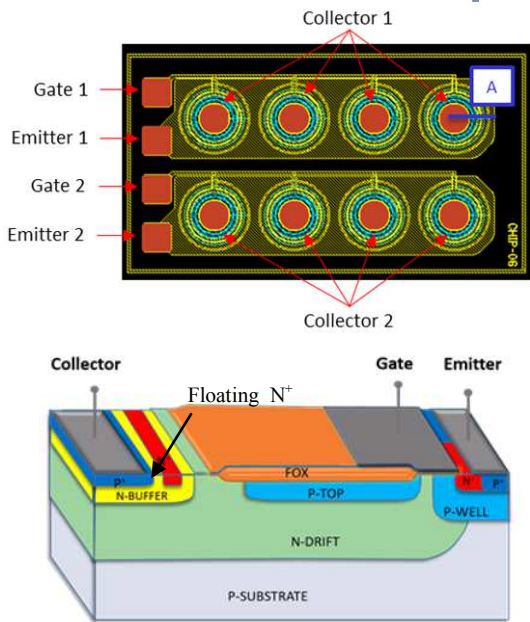


Fig.2: (a) Fabricated LIGBT in 0.6µm bulk silicon technology layout (b) 3D cross-section along A

next to collector P^+ [3]. This feature allows layout based tuning and minimisation of device losses based on the application. Based on this, an 800V LIGBT for high frequency, low-cost applications has been developed and implemented in low power high efficiency switch mode power supply (SMPS) systems[3]. This makes the LIGBT devices suitable for LED drivers.

II. PACKAGE THERMAL DESIGN

The temperature within LED lamps makes it imperative to have an effective thermal package design for the devices. Just as it is important to ensure that the temperature of the devices is kept within limits, it is also of importance to ensure the heat generation in the device doesn't significantly increase the ambient temperature. This is due to the fact that the LED optical output is significantly affected by the temperature as presented in [4, 5]. In [5] the optical output was measured while altering the ambient temperature. The results show that the higher the ambient temperature, the higher the number of non-radiative recombination of carriers and subsequently diminishing the light intensity [6, 7]. This emphasises the importance of a good thermal design.

Two possibilities were explored to package the LIGBT, the use of printed circuit boards (PCB) with modifications and the use of insulated metal substrate (IMS). The PCB package design for an effective cooling of the LIGBT is presented in Fig.3(a). The package is designed for optimal thermal performance using vias linking the device solder balls and top PCB copper layer to the base which can be used for cooling.

An additional copper foil is used as a heatsink to extract heat from the backside of the device and the PCB copper layer.

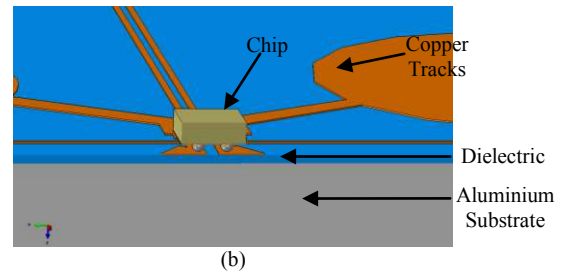
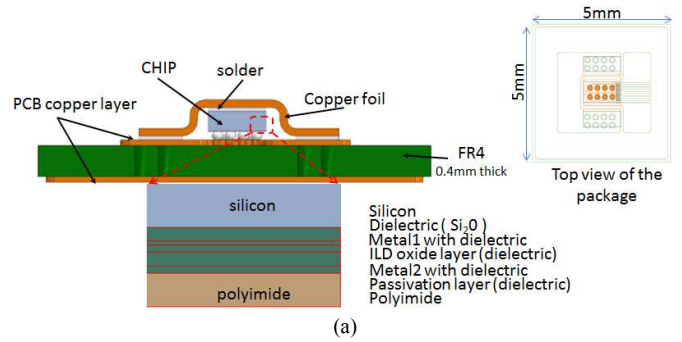


Fig.3: (a) PCB design for an effective cooling of LIGBT (b) IMS design for an effective cooling of LIGBT

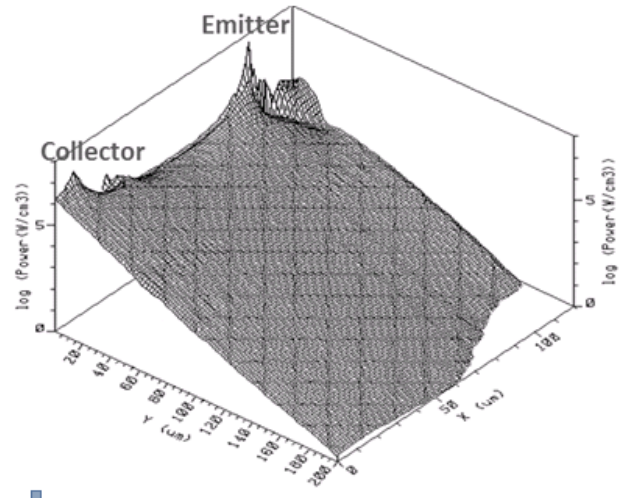


Fig.4: 3D plot of heat generation

Solder is used to attach the copper foil to the device backside to improve thermal performance. An alternative to PCB of reduced complexity is the insulated metal substrate (IMS) which is shown in Fig.3(b). The IMS consists of a copper layer which is used for electrical connection and also aids by conducting the heat generated by the device. A dielectric material of typical thickness of 100µm is used to isolate the copper tracks electrically from the aluminium substrate. The aluminium substrate can be used as a heatsink.

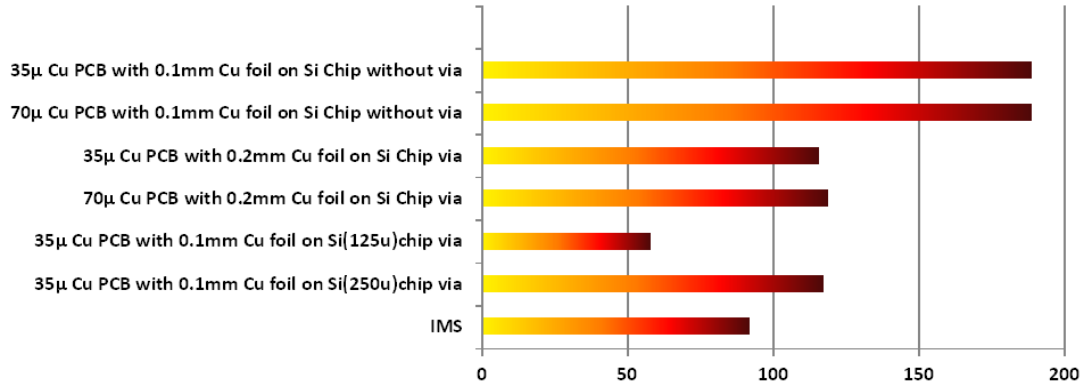
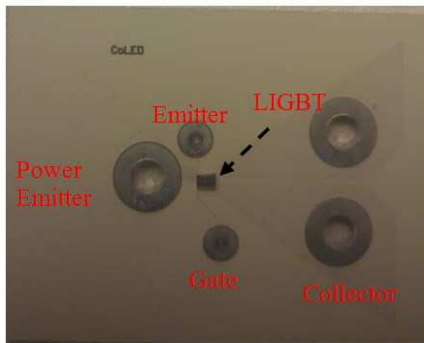
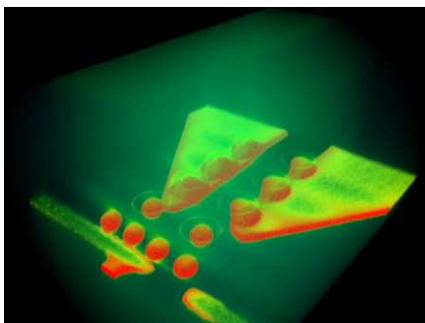


Fig.5: Steady state thermal simulation results on a linearly distributed body heat flux (applied across the thickness of silicon) for different packaging configurations showing the ΔT (between chip and ambient in $^{\circ}C$) for 1W power dissipation for 7W LED.

An extraction of the heat generation profile shows that heat generation is highest at the terminals and linearly decreases as it moves deeper away from the device terminals as shown in Fig.4. By applying the heat profile in finite element analysis (FEA), different packaging configurations have been analysed by including and varying vias, copper foil as heat sink and the thickness of the PCB copper track. The best thermal performance is achieved with 35 μm PCB copper thickness, 0.1 mm copper foil, chip thickness of 125 μm and the inclusion of vias as shown in Fig.5. For a chip thickness of 250 μm , the IMS produces the best thermal performance with a ΔT of 92 $^{\circ}C$. As a result, IMS is then chosen to create a prototype. The device is soldered on IMS using a die bonder by heating the IMS at 250 $^{\circ}C$ utilizing camera aids to align the pads to the balls accurately. The profile of the solder ball is presented in Fig.6 using X-ray imaging. This profile was used to simulate the electric field behaviour in section IV.



(a)



(b)

Fig.6: (a) Test sample soldered on IMS (b) X-ray image of the solder balls

III. THERMO-MECHANICAL MODELLING

Thermo-mechanical modelling of package structure of eight circle LIGBT device was undertaken in order to predict the strain and stresses in the solder. The package components consists of eight circle LIGBT device (device consist of aluminum metal layers, polyimide, SiO₂ and Si substrate as in Fig 3(a).

The solder viscoplastic properties were extracted from Cheng *et al* [8]. The standard temperature cycling with ramp and dwell time of 3 and 15 minutes with range of (-25, 125 $^{\circ}C$) was imposed on the model. The package structure was structurally restricted with three point structural boundary restriction constraint. Plastic strain distributions of solder were extracted from the numerical simulation. The plastic strain distribution of solder bump is shown in Fig 7. Accumulated plastic strain of solder bump, solder layer between copper foil and PCB, and the solder layer between copper foil and the silicon substrate were evaluated by volume weighted averaging of thin layer (10 μm) of the total volume. A Coffin Manson fatigue model [9] was utilised for lifetime estimation of solder joint. It was noted that solder layer between copper foil and the silicon substrate has the worst lifetime with 1797 cycles to failure. This highlights another advantage of using the IMS over the PCB package, as with the IMS no copper foil is required or additional solder is required.

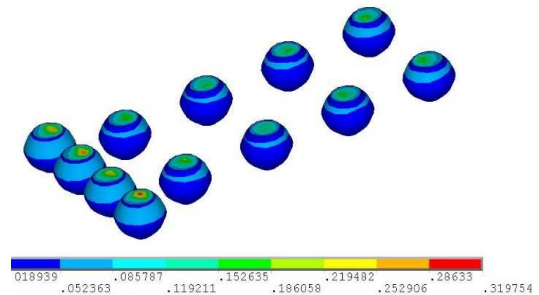


Fig.7: Plastic strain distribution on the solder bump

IV. UNDERFILL ELECTRIC FIELD MODELLING

The choice of under fill for flip-chip assembly is also important in the context of overall reliability. In order to

optimise overall package construction detailed finite element models have been built to assess electric field distributions in the underfill for ‘off’ state of the package structure. The governing equation (Poisson equation) of the electro-static analysis is

$$\begin{aligned} \nabla E &= \frac{\rho}{\epsilon} \\ \nabla \times E &= 0 \Rightarrow \nabla(\nabla V) = -\frac{\rho}{\epsilon} \\ E &= -\nabla V \end{aligned} \quad (1)$$

where E- electric field, V-electric potential, ϵ – permittivity of the medium, ρ - electric charge density. The material properties of device were sourced from public domain [10] for initial study. The permittivity values of underfill, solder (Sn3.5Ag), polyimide, SiO₂, aluminum, Si die are respectively 3.6, 2, 3.2, 3.9, 1.6, and 11.8. The high voltage (600V) was applied on the collector and solder bumps and ground voltage (0V) was applied on the gate of the device. Higher electric field distribution was concentrated in the region close to polyimide/solder/underfill interface as shown in Fig.8(c) and 9(c). For underfill relative permittivity value of 3.6 F/m, the maximum electric field vector sum value of 27.5 V/ μ m was observed in the modelling as in Fig 9 (a).

vector sum value of 27.5 V/ μ m was observed in the modelling as in Fig 9 (a). Two of the commercial underfill (manufactured by Henkel [11]) such as Loctite 3565 and Loctite 3563 are capable of withstanding dielectric breakdown failure to the extreme electric fields generated in the FEA model.

V. CONCLUSION

This work has presented different packaging solutions and identified a suitable package to ensure reliable operation of IGBT devices for in LED driver applications. Thermal simulations and electrostatic simulations have been presented to validate this approach.

ACKNOWLEDGEMENT

The authors would like to express their gratitude to the EPSRC Centre for Power Electronics-UK for support and their interest in lateral technologies.

REFERENCES

- [1] T. Trajkovic, N. Udugampola, V. Pathirana, F. Udrea, J. Smithells, and T. Wotherspoon, "Flip-chip assembly and 3D stacking of 1000V lateral IGBT (IGBT) dies," in *2016 28th International Symposium on Power Semiconductor Devices and ICs (ISPSD)*, 2016, pp. 139-142.
- [2] G. Camuso, N. Udugampola, V. Pathirana, T. Trajkovic, and F. Udrea, "Avalanche ruggedness of 800V Lateral IGBTs in bulk Si," in *2014 16th European Conference on Power Electronics and Applications*, 2014, pp. 1-9.
- [3] T. Trajkovic, N. Udugampola, V. Pathirana, G. Camuso, F. Udrea, and G. A. J. Amaratunga, "800V lateral IGBT in bulk Si for low power compact SMPS applications," in *2013 25th International Symposium on Power Semiconductor Devices & IC's (ISPSD)*, 2013, pp. 401-404.
- [4] C. De Santi, M. Dal Lago, M. Buffolo, D. Monti, M. Meneghini, G. Meneghesso, and E. Zanoni, "Failure causes and mechanisms of retrofit LED lamps," *Microelectronics Reliability*, vol. 55, pp. 1765-1769, 2015.
- [5] M. E. Raypah, M. Devarajan, and F. Sulaiman, "Modeling Spectra of Low-Power SMD LEDs as a Function of Ambient Temperature," *IEEE Transactions on Electron Devices*, vol. 64, pp. 1180-1186, 2017.
- [6] D. G. Todorov and L. G. Kapisazov, "LED thermal management," presented at the in Proc. Electron, 2008.
- [7] A. Groh, S. Brückner, and T. Q. Khanh, "The temperature-dependent changes of the photometrical and colorimetical parameters of today high power LEDs," in *7th Int. Symp. Auto-Motive Lighting*, Munchen, 2007, pp. 622–629.
- [8] Z.N. Cheng, G.Z. Wang, L. Chen, J. Wilde, and K. Becker, "Viscoplastic Anand model for solder alloys and its application," *Soldering & Surface Mount Technology*, vol. 12, pp. 31 - 36, 2000.
- [9] C. Andersson, Z. Lai, J. Liu, H. Jiang, and Y. Yu, "Comparison of isothermal mechanical fatigue properties of lead free solder joints and bulk solders," *Mater. Sci. Eng. A*, vol. 394 pp. 20–27, 2007.
- [10] T. Siewet, S. Lie, D. R. Smith, and J. C. Madeni, "Properties of lead-free solders," vol. Release 4.0, ed. National institute of standards (NIST) and Colorado School of mines, 2002.
- [11] H. L. Corporation. Available: <http://www.henkel-adhesives.com>

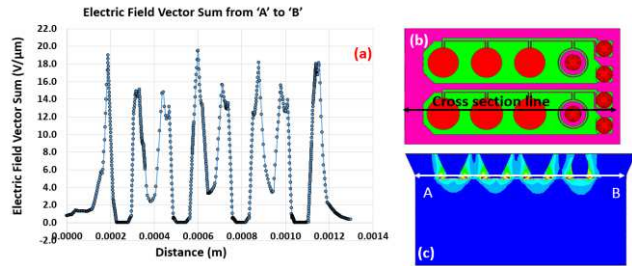


Fig 8: (a) Electric field vector sum versus distance from ‘A’ to ‘B’ across the solder bumps with 203.7 μ m PCB opening, (b) Top view of the cross section line, (c) electric field vector sum distribution on the side view

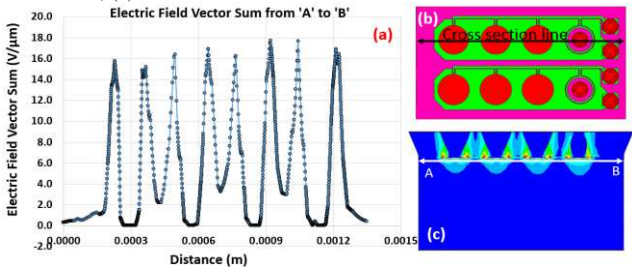


Fig 9: (a) Electric field vector sum versus distance from ‘A’ to ‘B’ across solder bumps with 192.3 μ m PCB opening, (b) Top view of the cross section line, (c) electric field vector sum distribution on the side view

Two solder bump dimensions ((1) width (base) of 41.6 μ m, and PCB opening of 192.3 μ m, and (2) width (base) 57.2 μ m, and PCB opening of 203.7 μ m) measured in the experiment were modelled for electric static analysis. It was noted that the underfill region around the larger solder bump exhibit higher electric field distribution as in Fig 9 (a) and 10 (a). In addition, increase in relative permittivity value decreases the electric field in the underfill. If the maximum electric field is less than dielectric strength of the underfill then the underfill can withstand the breakdown failure. The maximum electric field